JCI The Journal of Clinical Investigation

Tetracycline-induced mitohormesis mediates disease tolerance against influenza

Adrienne Mottis, … , Mark L. Nelson, Johan Auwerx

J Clin Invest. 2022. https://doi.org/10.1172/JCI151540.

Research In-Press Preview **Infectious disease**

Mitohormesis defines the increase in fitness mediated by adaptive responses to mild mitochondrial stress. Tetracyclines inhibit not only bacterial but also mitochondrial translation, thus imposing a low level of mitochondrial stress to eukaryotic cells. We demonstrate in cell and germ-free mouse models, that tetracyclines induce a mild adaptive mitochondrial stress response (MSR), involving both the ATF4-mediated integrative stress response and type I interferon (IFN) signaling. To overcome the interferences of tetracyclines with the host microbiome, we identify tetracycline derivatives that have minimal antimicrobial activity, yet retain full capacity to induce the MSR, such as the lead compound, 9-tert-butyldoxycycline (9-TB). The MSR induced by Doxycycline (Dox) and 9-TB improves survival and disease tolerance against lethal influenza virus (IFV) infection when given preventively. 9-TB, unlike Dox, did not affect the gut microbiome and showed also encouraging results against IFV when given in a therapeutic setting. Tolerance to IFV infection is associated with the induction of genes involved in lung epithelial cell and cilia function, and with down-regulation of inflammatory and immune gene sets in lungs, liver, and kidneys. Mitohormesis induced by non-antimicrobial tetracyclines and the ensuing IFN response may dampen excessive inflammation and tissue damage during viral infections, opening innovative therapeutic avenues.

Title: Tetracycline-induced mitohormesis mediates disease tolerance against influenza

Authors: Adrienne Mottis [1], Terytty Yang Li [1], Gaby El Alam [1], Alexis Rapin [1], Elena Katsyuba [1,2], David Liaskos [2], Davide D'Amico[1], Nicola Laraine Harris [3,4], Mark C. Grier [5], Laurent Mouchiroud [2], Mark L. Nelson [5], Johan Auwerx [1,#]

Affiliations:

1 Laboratory of Integrative Systems Physiology, Institute of Bioengineering, Ecole Polytechnique Fédérale de Lausanne, CH-1015 Lausanne, Switzerland

2 Nagi Bioscience SA - EPFL Innovation Park, CH-1024 Ecublens, Switzerland

3 Laboratory of Intestinal Immunology, Global Health Institute, Ecole Polytechnique Fédérale de Lausanne, CH-1015 Lausanne, Switzerland

4 Department of Immunology and Pathology, Central Clinical School, Monash University, Melbourne, VIC 3004, Australia.

5 Echelon Biosciences, Inc., Salt Lake City, UT 84108, USA

Correspondence should be addressed to J.A. **(**admin.auwerx@epfl.ch)

Conflict of interest statement:

AM, MN, and JA are inventors on patent application covering this work filed by the EPFL. LM, EK and DL are employed by Nagi Bioscience. LM and JA have equity interest in Nagi Bioscience SA.

One sentence summary: Low levels of mitochondrial stress induced by non-antimicrobial tetracyclines enable survival and tolerance to influenza infection in mice

Abstract:

Mitohormesis defines the increase in fitness mediated by adaptive responses to mild mitochondrial stress. Tetracyclines inhibit not only bacterial but also mitochondrial translation, thus imposing a low level of mitochondrial stress to eukaryotic cells. We demonstrate in cell and germ-free mouse models, that tetracyclines induce a mild adaptive mitochondrial stress response (MSR), involving both the ATF4-mediated integrative stress response and type I interferon (IFN) signaling. To overcome the interferences of tetracyclines with the host microbiome, we identify tetracycline derivatives that have minimal antimicrobial activity, yet retain full capacity to induce the MSR, such as the lead compound, 9-tert-butyldoxycycline (9-TB). The MSR induced by Doxycycline (Dox) and 9-TB improves survival and disease tolerance against lethal influenza virus (IFV) infection when given preventively. 9-TB, unlike Dox, did not affect the gut microbiome and showed also encouraging results against IFV when given in a therapeutic setting. Tolerance to IFV infection is associated with the induction of genes involved in lung epithelial cell and cilia function, and with down-regulation of inflammatory and immune gene sets in lungs, liver, and kidneys. Mitohormesis induced by non-antimicrobial tetracyclines and the ensuing IFN response may dampen excessive inflammation and tissue damage during viral infections, opening innovative therapeutic avenues.

List of abbreviations:

9-TB: 9-tert-butyl-doxycycline
ARDS: acute respiratory distress syndrome
ATc: anhydrotetracycline
BMDM: bone marrow-derived macrophages
DAMP: damage-associated molecular pattern
Dox: doxycycline
GSEA: gene set enrichment analysis
GO: gene ontology
IFN: interferon
IFV: Influenza virus
ISG: interferon-stimulated gene

ISR: integrated stress response
OXPHOS: oxidative phosphorylation
MEF: mouse embryonic fibroblast
MODS: multiorgan dysfunction syndrome
MSR: mitochondrial stress response
mtDNA: mitochondrial DNA
NMDS: non-metric multidimensional scaling
perMANOVA: permutational multivariate analysis of variance
PBMC: peripheral blood mononuclear cell
SARS-CoV2: severe acute respiratory syndrome coronavirus 2
SDI: Shannon diversity index
Tet: tetracycline
TFAM: Transcription Factor A Mitochondrial
UPR^{mt}: mitochondrial unfolded protein response

Introduction

Cells constantly monitor the function of their mitochondria and activate adaptive mitochondrial stress responses (MSR) to maintain or restore mitochondrial homeostasis upon stress. Mitohormesis is the phenomenon that ensues when these adaptive responses surpass the initial stress and lead to overall beneficial consequences on cellular and organismal fitness. A prototypical and well-studied form of the MSR is the mitochondrial unfolded protein response (UPR^{mt}), first described in mammalian cells (1), but more extensively characterized in *Caenorhabditis elegans* (*C. elegans*) (reviewed in (2–4)). Fitting with a beneficial health impact, the mitohormetic induction of the MSR is reported to extend health- and lifespan in *C. elegans* (5, 6), as well as to attenuate the phenotypic consequences of Alzheimer's disease and exert cardioprotective effects in mouse models (7, 8). Interestingly, Tetracyclines (Tets) - antibiotics that not only block bacterial, but also mitochondrial translation - can be used to induce such a mild proteotoxic mitochondrial stress. Tets are therefore pharmacological tools that induce the MSR (7, 9), often resulting in a beneficial mitohormetic response.

Mitochondrial function and immunity, both innate and adaptive, are interconnected at multiple levels (10, 11). Mitochondrial metabolism is a central determinant of the type and course of immune response, and damaged mitochondria contribute to inflammation through the release of damage-associated molecular patterns (DAMPs) amongst other mechanisms (12). In addition, mitochondria can be targeted by multiple bacterial as well as viral infections (13). Mitochondrial function has been proposed to be essential to trigger tolerance to infection (14, 15). Resistant hosts fight infection by eliciting an immune response that reduces pathogen load, whereas tolerance refers to

the mechanisms that limit the extent of organ dysfunction and tissue damage caused by infection, not necessarily impacting on pathogen load (16).

Respiratory viruses such as Influenza A virus (IFV) or SARS-CoV2 represent a major public health concern as our aging population is highly susceptible to the complications and often lethal consequences of such infections (17). Uncontrolled systemic inflammation ensuing from infection by respiratory viruses can lead to acute respiratory distress syndrome (ARDS) and multiorgan dysfunction syndrome (MODS), which are both in part driven by mitochondrial dysfunction (18, 19), contributing significantly to complications and mortality.

We here explore the potential of Tets to induce mitohormesis and disease tolerance within the context of respiratory infection caused by IFV. To dissociate the impact of Tets on the microbiome from potential effects on mitohormesis and tolerance, we profiled the transcriptomic response to doxycycline in germ-free mice and show that the Tet-induced MSR crosstalks with the innate immune system, in particular with type I interferon (IFN) signaling. We then assess and select Tet derivatives, devoid of antibacterial activity, for their ability to trigger the MSR in worms and cells. We finally provide proof-of-concept that a non-antibacterial Tet, substituted at the C9 position, named 9-tert-butyl-doxycycline (9-TB), induces disease tolerance and increases the survival of mice infected with a lethal dose of IFV by lowering systemic and local inflammation, and limiting lung tissue damage, without affecting the gut microbiome.

Results

To characterize the MSR induced by Tets in vivo, we administered doxycycline (Dox) at 500 mg/kg/day (mpkd) in the drinking water to 9 weeks-old germ-free C57BL/6J mice for 16 days (5, 7), hence eliminating the potential confounding impacts of Dox on the microbiome. Body weight at the time of the sacrifice was not different between the control and Dox-treated animals (Fig. S1A), indicating the absence of obvious adverse effects. As reported in livers of mice maintained under conventional conditions (9), OXPHOS complex activity as well as ATP levels were also reduced by Dox in kidneys of germ-free mice (Fig. 1A). Dox elicited organ-specific transcriptional responses, with the expression of quantitavely more and qualitatively different genes being affected in the kidney and different ones compared to the liver (Fig. S1B-C, Table S1). In Dox-treated kidneys, gene set enrichment analysis (GSEA) (20) revealed the induction of the ATF4-mediated integrated stress response (ISR) (Fig. 1B), a common hallmark of the mammalian MSR (21). The MSR features the induction of mitochondrial chaperones and proteases, such as *Hspa9* and *Lonp1*, as well as of enzymes mediating adaptation to nutrient deprivation, such as asparagine synthetase (ASNS), which were increased at both the transcript and protein levels (Fig. 1C-D, S1D). In line with the activation of the ATF4-ISR pathway, the kidney displayed increased eIF2α phosphorylation (Fig. 1E, S1E), which slows down cytosolic cap-dependent translation as a compensation for energy deprivation caused by mitochondrial stress and favors the translation of ATF4 transcripts by cap-independent mechanisms (22). Kidneys of the Dox-treated germ-free mice thus gathered the typical attributes of the ATF4-ISR pathway, a hallmark of the mammalian response to mitochondrial stress.

In the liver, eIF2α phosphorylation and the ATF4-ISR program were not induced (Fig. S1F-G, Table S2). The liver transcriptome, however, indicated that Dox induced the

type I IFN response (Fig. 1F-G), which was confirmed at the protein level by the increased expression of two interferon-stimulated genes (ISGs), Cyclic AMP-GMP synthetase (CGAS) and C-X-C motif chemokine ligand 10 (CXCL10), and the increased phosphorylation of TANK-binding kinase 1 (TBK1) (Fig. 1H, S1H). The type I IFN response is an innate immune pathway that, upon sensing viral DNAs, activates cGAS-STING-TBK1 signaling, culminating in the secretion of the type I IFNs, IFNα and IFNβ, and the induction of the expression of ISGs (23). Of note, the type I IFN response was also induced in kidneys but to a lesser extent (Fig. S1I-J-, Table S2).

Similarly in mouse bone marrow derived macrophages (BMDM), a highly relevant model to investigate innate immune signaling in vitro, Dox induced the expression of ISGs and triggered the phosphorylation of TBK1 (Fig. 1I-J, S1K). mtDNA effusing from the mitochondria into the cytosol was shown before to elicit the type I IFN response in the context of mitonuclear genomic instability caused by the loss of function of Transcription Factor A Mitochondrial (TFAM) (12). We also detected increased levels of mtDNA in the cytosol of Dox-treated BMDMs (Fig. 1K), which underpins the activation of antiviral signaling resulting in the secretion of IFNβ from these BMDMs (Fig. 1L). Finally, Dox-induced secretion of IFNβ was abrogated by the nucleoside analogue, 2',3'-dideoxycytidine (ddC) (Fig. 1L), which gradually leads to depletion of mtDNA (24), demonstrating that cytosolic release of mtDNA contributes to the activation of antiviral signaling.

We then set out to identify tetracyclines with lower antimicrobial activities that could be easier developed for clinical use. To this effect, we screened in *C. elegans* a library of 52 position-modified Tet derivatives that are clinically used, are synthetic intermediates, or derivatives specifically synthesized to probe initial structure-activity relationships (SAR) amongst Tets that elicit the MSR (Fig. 2A-C), most of them having

very limited antibacterial activity (Table 1). We screened the compounds for induction using a *C. elegans hsp-6::gfp* reporter strain with Dox administration and *cco-1* RNAi feeding as positive controls, as previously described (25) (Fig. 2C). Out of the 52 Tet derivatives tested, representing clinically relevant and C2-C10 position modified compounds (26–32) (Fig. 2A-B), we identified 9-tert-butyl-doxycycline **1** (9-TB) and anhydrotetracycline **2** (ATc), as the strongest activators of the UPR^{mt} (Fig. 2C). We then compared detailed dose-responses of Dox, 9-TB, and ATc to induce a GFP signal in the *C. elegans hsp-6::gfp* reporter strain in an automated microfluidic device (33). 9-TB and ATc were again in this system more efficacious at lower doses to induce the UPR^{mt} relative to Dox (Fig. 2D, S2A), with 9-TB surpassing the robust UPR^{mt} activation caused by *cco-1* RNAi feeding (Fig. 2C-D).

In addition, other derivatives modified along the upper periphery spanning positions C2, C4, C5, C6, C13 and aromatic positions C7-C9 also activated the UPR^{mt}, such as compounds **3-5**, although their effect was not as pronounced as that of 9-TB and ATc (Fig. 2A-B). In contrast, clinically used minocycline **7**, Nuzyra^{TM} **14** (see Table S3), Tygacil^{TM} **23** or derivatives based on the minocycline scaffold did not activate the UPR^{mt} (16 compounds), while C5-C-9 derivatives of sancycline only mildly activated the UPR^{mt} (see Table S3). Additionally, compounds modified at the lower periphery, spanning positions C10, C11, C12-C1, and the A-ring C2 carboxamide did not induce the activity of the GFP reporter, showing the importance of this integrated phenolic keto-enol system in maintaining UPR^{mt} activity (34, 35).

We then characterized the pharmacology of Dox, 9-TB and ATc in human embryonic kidney (HEK) 293T cell line. 9-TB and ATc also generated a more robust MSR response than Dox, as reflected by their impact (up to almost 2-fold stronger) on the mitonuclear protein imbalance (Fig. 3A), a disbalanced ratio between mitochondrial-

versus nuclear-encoded OXPHOS subunits, underpinning the induction of the MSR (5). Furthermore, 9-TB and ATc reduced basal oxygen consumption rate (OCR) in a dose-dependent and more pronounced fashion than Dox (Fig. 3B). The induction of transcripts for the mammalian MSR signature genes, was likewise more prominent with 9-TB and ATc (Fig. 3C). In mouse BMDMs, lower doses of 9-TB (1.88 µg/ml) and ATc (3.75 and 7.5 µg/ml) were also superior to Dox (at 7.5 and 15 µg/ml) to induce the ISGs and MSR genes (Fig. 3D, S3A) and the secretion of IFNβ (Fig. 3E). Knocking-out ATF4 in mouse embryonic fibroblasts (MEFs) showed that Tets induced the MSR and most ISGs genes in an ATF4-dependent manner (Fig. S3B). Taken together, these studies in *C. elegans*, mouse BMDMs, human HEK293T cells and MEFs cells ascertained the identification of non-antimicrobial Tets with higher potency to trigger the MSR and type I IFN response, relative to our benchmark anti-bacterial Tet, Dox.

mtDNA instability-driven innate immunity can potentiate resistance to viruses (12) and mediates the antiviral immune response against the IFV (36). We thus asked whether the Tet-induced MSR enables mice to survive infection by IFV. We hence subjected 8 week-old female BALB/cN mice to either mock (1 group, n=10) or intranasal inoculation with 175 PFU of the IFV H1N1 PR8 strain (3 groups). The 3 infected groups (n=10 each) were given vehicle, Dox (at 40 mpkd) or 9-TB (at 1 mpkd) by daily intraperitoneal injection, from day -3 pre-inoculation (Fig. S4A). Dox and 9-TB improved the survival to the infectious challenge, with 50% of the mice treated with respectively Dox or 9-TB recovering (Fig. 4A). The improved health of the Tet-treated cohorts was further supported by the recovery of body weight loss, and their improved clinical score (Fig. 4B, S4C). In contrast, the IFV infection was lethal to all control mice by day 11 post inoculation. Strikingly, at day 7 post infection no significant difference in viral titer in the lung tissue was observed (Fig. 4C). Similarly, when mice were infected with a much

higher viral load (1000 PFU; Fig. S3B), Dox and 9-TB delayed mortality and the decline in health (Fig. 4E-F, S4E), again in the absence of an impact on the viral titer in the lungs at day 5 post-infection (Fig. 4G). The Tet-induced MSR did not cause obvious adverse effects (Fig. S4D), yet decreased the levels of Interleukin 6 (IL-6) in both 175 and 1000 PFU experiments (Fig. 4D, 4H), and of some other markers of tissue stress and damage (Fig. S4F) (37–39). These results demonstrate that the Tet-induced MSR increases the survival of mice to a lethal IFV by improving tolerance, rather than by reducing viral load, which is reflective of resistance to the virus.

To assess the impact of Tets on the microbiome we transiently single-caged animals and longitudinally collected feces before (Day -4 pre-IFV-inoculation), 3 days after (Day 0, just before IFV-inoculation) and 6 days after (Day 3, post- IFV-inoculation) the start of daily administration of 9-TB, respectively Dox. We then extracted DNA from feces and performed whole metagenome sequencing. While the composition and diversity of the bacterial communities showed no differences between groups before treatment, the gut bacterial community of mice treated with Dox showed a significant difference in composition compared to both untreated mice and mice treated with 9-TB both after 3 and 6 days of tetracycline treatment (respectively Day 0 and Day 3 post-inoculation), as assessed by permutational multivariate analysis of variance (perMANOVA) and visualized by non-metric multidimensional scaling (NMDS) (Fig. 5A and Table S8). This was reflected by a lower bacterial species diversity in Dox-treated mice both in terms of Shannon diversity index (SDI) and richness (Fig. 5B). In contrast, no differences were observed between 9-TB treated mice and untreated mice at any time point, suggesting that that the administered dose of 9-TB does not affect the mice gut microbiota in vivo (Fig. 5A, 5B and Table S8).

To further investigate the clinical relevance of novel Tet derivatives we focused on 9-TB and administered 9-TB in a therapeutic mode starting at Day 1 post-inoculation of 760 PFU of the IFV H1N1 PR8 strain (Fig. S5A). Of note, the different death kinetics and survival proportion with regard to the high viral load (760 PFU) in Fig. 5C-5D and Fig. S5A-S5D in comparison with Fig. 4A and 4E at lower viral load (175 PFU) are due to the fact that both experiments were run with different viral batches. Nevertheless, although not significant, the trend of 20% survival upon administration of two very low doses of 9-TB (0.025 and 0.05 mpkd) are highly encouraging (Fig. 4C-4D) and suggest that novel Tets derivatives can trigger tolerance to IFV in a clinically relevant setting. Future investigations are thus needed to optimize the timing and doses of Tet derivatives and refine their therapeutic potential in viral infections.

To gain insight into the mechanisms underlying the Tet-induced disease tolerance, we analyzed the transcriptomes of the lung, as well as of liver and kidney (Fig. S6A), 2 organs often affected by the multi-organ failure syndrome seen after infection by respiratory viruses like IFV or SARS-CoV2 (40). In each tissue, principal component analysis (PCA) separated non-infected from IFV infected mice along the first dimension, PC1, whereas 9-TB had a more pronounced and less variable effect, with better clustering and further separation, along the second dimension relative to control and Dox transcriptomes (Fig. 6A, S6B).

GSEA showed that 9-TB significantly down-regulated multiple inflammatory and immune-related terms in the lungs (Fig. 6B, S6D), such as “immune response”, “t cell activation” or “b cell activation”. We then sought to characterize how 9-TB reversed the effect of IFV infection on transcript levels (Fig. S6A). We thus assessed which Gene Ontology (GO) Biological Processes (GOPB) terms were enriched in the intersection of gene sets changed in opposite directions by infection and 9-TB, respectively (Fig.

S6C). As summarized by Revigo representation (41) (Fig. S6A), inflammatory, immune and apoptotic processes were the main enriched terms amongst genes induced by IFV and down-regulated by 9-TB (Fig. 6C, left panel). Infection by IFV leads to lung epithelial cell dysfunction and down-regulation of genes implicated in cilia or tight junctions, which underpin failures of muco-ciliary clearance and barrier function that contribute to the pathogenesis of ARDS (19). Accordingly, multiple gene sets related to lung development and to lung cell function and structure were decreased by IFV infection and their expression was restored by 9-TB (Fig. 6B, S6E, 6C, right panel). Altogether, 9-TB elicits disease tolerance to IFV mainly by counteracting inflammation and the loss of lung epithelial cells and structures, processes that directly determine the severity of infection by respiratory viruses.

To estimate the impact of the infectious challenge or Tet treatment on the lung cell types, we used single-cell RNA-Seq (scRNA-Seq) transcriptomic profiles of mouse (42) and human (43) lung cell populations from 2 independent studies studying IFV infection; one of these studies furthermore established cell markers that overlap between mouse and human lung cell types (43). Using these cell profiles to perform GSEA on our data confirmed that 9-TB reverted the loss of multiple cell types crucial to lung function, such as club, ciliated and alveolar epithelial cells (Fig. 6D), whereas it decreased several classes of immune cells, such as neutrophils, natural killer cells and monocytes, all contributing to tissue damage upon IFV infection (17). Dox showed similar, but more discrete, tendencies towards changes in cellular patterns (Fig. 6D). These observations were confirmed when using a different set of scRNA-Seq cell profiles on IFV infected mouse lungs (Fig. S7A) (42).

9-TB also down-regulated multiple immune-related and inflammatory gene sets in liver and kidney (Fig. S7B). In particular, as shown through Revigo analysis, these immune

and inflammatory terms were enriched amongst the group of liver genes induced by IFV and down-regulated by 9-TB (Fig. S7C-D). In the 3 organs studied, Dox was leading to a weaker down-regulation of many of these terms as shown by GSEA (Fig. S7B), suggesting that it does not lower systemic IFV-driven inflammation as efficiently as 9-TB, which is also consistent with its more moderate impact on IL-6 plasma levels (Fig. 4D). On top, Dox induced gene sets involved in cytopathic processes and fibrogenesis in liver and kidney (Fig. S7B), suggesting an improved safety profile of the 9-TB, relative to Dox, at doses showing similar efficacy. Further investigations will be needed to establish whether the relative up-regulation of extracellular matrix/collagen gene sets by 9-TB in lungs (i.e. the site of highest tissue damage due to the infectious challenge) corresponds to proper healing and tissue repair mechanisms (Fig. S7). Taken together, our transcriptomic data highlight that Tet-induced mitohormesis (and in particular 9-TB), elicits disease tolerance to IFV by preventing IFV-associated lung damage and by dampening inflammatory responses not only in lungs, but in liver and kidney as well.

Discussion

Here we report that Tets can be used to safely induce an adaptive mitohormetic response, leading not only to the activation of the ATF4-ISR pathway, but also to the induction of type I IFN signaling in vitro and in germ-free mice. This translates into a beneficial impact on lethal IFV infection, where Tets enabled survival and induced disease tolerance of infected mice. RNAseq data from lung, liver, and kidney helped to unveil the mechanisms underlying tolerance to IFV infection. Tets rescued the transcript levels of genes involved in lung epithelial cell function and implicated in cilia or tight junctions, which are often found downregulated upon viral respiratory infections as a result of lung damage (19). On the contrary, Tets systematically down-regulated multiple inflammatory and immune related gene sets in the lung, liver, and kidney transcriptome data (Fig. 6B-C, S7B, S7D). Enrichment of cell profiles based on scRNA-Seq suggested that Tets attenuated the loss of club, ciliated and alveolar epithelial cells in the lungs, while reducing immune cell infiltration (Fig. 6D). We also ascertained a robust reduction of IL-6 (Fig. 4D, H) and of other markers of inflammation and tissue damage (Fig. S4D). We furthermore demonstrate that non-antimicrobial tetracyclines, such as 9-TB, do not cause disturbances of the microbiome upon treatment in vivo in mice as shown by profiling bacterial species in longitudinally-collected feces (Fig. 5A, 5B). We finally provide highly encouraging results suggesting that even 9-TB administered therapeutically 1 day post inoculation with IFV can increase survival, supporting the clinical relevance of the study. Although the detailed doses and kinetics of the treatments and the immune response to IFV remain to be investigated, we speculate that a possible mechanism for Tet-induced mitohormesis may involve a mild boost of the IFN response early after treatment, leading to overall favorable consequences on inflammation and tissue damage (44), as explained below.

An important limitation for the use of Tets, which inhibit both the bacterial and hence also the mitochondrial translation, comes from their anti-microbial activity that influences the host microbiome. Using a primary screening that identified compounds based on the induction of the UPR^{mt} in *C. elegans*, combined with the analysis of their anti-microbial activity, we identified a series of candidates through preliminary SAR that have no or very weak antimicrobial activity, yet retain full or even superior capacity to induce the MSR. Indeed, lower doses of 9-TB and ATc led to the induction of the MSR in vitro and to disease tolerance in vivo; these compounds were devoid of some of the adverse effects of Dox (Fig. S7). On top, at the doses required, 9-TB had no detectable effect on the composition and diversity of the gut bacterial communities as assessed by whole metagenome sequencing on longitudinally collected mice feces, while Dox did (Fig 5A, 5B and Table S8). This confirms that 9-TB can target mitochondria while not affecting commensal bacteria, both ruling out the hypothesis that the observed effects may be partly mediated by a direct impact on the microbiome, and providing additional evidence for its target specificity (Fig. 5A, 5B and Table S8). This also indicates that one can select Tet derivatives for their enhanced activity on the mitobiome *versus* the microbiome and thereby dial out some adverse effects of the Tets.

Mild levels of mitochondrial damage or dysfunction have the potential to activate type I IFN or other immune pathways, leading to inflammation (45). We also highlight this inverse relationship between mitochondrial function and type I IFN signaling in Dox-treated livers, kidneys and BMDMs (Fig. 1A-L, S1F-G). It hence appears logical that immune and mitochondrial quality control pathways are co-regulated in interlocked feedback circuits to prevent mitochondrial damage upon inflammatory triggers and vice versa. In line with this, a similar anti-correlation between mitochondria-encoded genes,

a proxy for both mitochondrial content and functionality, and type I IFN genes was reported in multiple cell types (46, 47), including in IFV-infected mouse lung cells analyzed by single-cell RNA-Seq profiling (42). This also indicates that moderate mitochondrial stress could be adaptive and trigger the induction of low levels of type I IFN that are beneficial (48). Indeed, a finely tuned IFN response allows a balanced immune response with optimal protection and minimal tissue damage, limiting the detrimental effects of a persistent IFN response (49). As an example, in COVID-19, endogenous high levels of type I IFN are protective (50) and early administration of IFNα decreased mortality, while late administration of IFNα increased mortality (51); this is consistent with the fact that delayed or chronic IFN responses disrupt lung repair and induce immunopathology (52, 53), while early administration of type I IFN is protective in influenza and coronaviruses infections (49, 53). Deciphering how exactly such moderate type I IFN response is coupled to a beneficial effect on inflammatory status and disease progression is thus particularly challenging given the dual nature of the immune-modulatory functions of type I IFN. Future investigations will have to determine how mitochondrial quality control and innate immune pathways mechanistically combine to translate into Tet-induced disease tolerance to IFV and potentially other viral infections. The ensuing insight may not only open new therapeutic avenues to cope with infections by respiratory viruses, but also to manage other diseases typified by mitochondrial dysfunction and inflammation, such as neurodegenerative (e.g. Alzheimer's (54)) and cardiovascular diseases (e.g. aortic aneurism (55)).

Methods

Mouse experiments in C57BL/6J mice

Male 9 weeks-old C57BL/6J mice were treated for 16 days with 500 mg/kg/day doxycycline hyclate (Sigma) in drinking water. All animals used in the experiments were randomly assigned to experimental or control groups. Mice were housed with ad libitum access to water and food and kept under a 12-hour dark/12-hour light cycle. As doxycycline is bitter, we supplemented the water for both conditions (treatments and controls) with 50 g/L sucrose. Drinking water was changed every 48 hours. Germ-free C57BL/6J mice were obtained from the Clean Mouse Facility, University of Bern (Bern, Switzerland), and compared with specific pathogen-free (SPF) C57BL/6J mice from Janvier Labs. All animal experiments were carried out according to the institutional, national Swiss and EU ethical guidelines and were approved by the local animal experimentation committee of the Canton de Vaud.

IFV infection in BALB/cN

8 weeks-old female mice were inoculated on day 0 with influenza virus A (Influenza A/PR/8/34 (H1N1) originating from ATCC VR-1469) via intranasal route at the amount of 175 PFU/mouse/50µL, 1000 PFU/mouse/50µL or 760 PFU mouse/50uL pending on the batch of the virus (Fig. S4A-B, S5A, S5C), under anesthesia by IP injection of anesthetic (Zoletil 50 at 30 mg/kg+Xylazine at 6 mg/kg). All animals used in the experiments were randomly assigned to experimental or control groups. Mice in all groups were treated with vehicle (saline) or the indicated concentrations of Dox/9-TB by intraperitoneal injection from day -7, day -3 for the preventive treatment or from day 1 for the therapeutic treatment until death/sacrifice (Fig. S3A, S3B). Body weight was monitored during the whole study. Body temperature, food intake (daily consumption in each cage) and clinical score were monitored from day 0 until death/sacrifice. For

each treatment/control group, 10-12 mice were followed for survival and 5-6 mice were sacrificed at day 7 (respectively day 5) for blood and organ collection. Blood samples were collected in tubes via cardiac puncture and anticoagulated by K_2EDTA, then centrifuged at 7000 g, 4 °C for 10 minutes to obtain plasma samples. Any mouse suffering from ≥35% body weight loss relative to day 0 was euthanized and counted as dead. Mice were blindly scored on a daily basis as follows: 1 = healthy mouse; 2 = mouse showing signs of malaise, including slight piloerection, slightly changed gait and increased ambulation; 3 = mouse showing signs of strong piloerection, constricted abdomen, changed gait and periods of inactivity; 4 = mouse with enhanced characteristics of the previous grade, but showing little activity and becoming moribund; 5 = mouse found dead. The study was performed by WuXi AppTec (Shanghai) Co., Ltd. according to the protocol following the institutional guidelines of Institutional Committee Animal Care and Use Committee, Shanghai Site (IACUC-SH) and approved by the Shanghai Science and Technology Committee (STCSM, Ministry of Science and Technology, PR of China).

HEK293T culture and oxygen consumption rate

HEK293T (Human embryonic kidney 293T) cells were purchased from ATCC and have been routinely checked in the laboratory for mycoplasma contamination with the MycoProbe detection kit (R&D systems). HEK293T were grown at 37 °C in a humidified atmosphere of 5% CO_2/95% air in DMEM medium with 4.5 g/L glucose (Gibco) including 10% FBS (Gibco), 1× nonessential amino acids (Invitrogen) and 5 mM penicillin/streptomycin (Invitrogen). Cells were treated for 24h with the indicated doses of compounds 24 hours after seeding. Oxygen consumption rate was measured with the Seahorse XF96 instrument (Seahorse Bioscience) according to the manufacturer's protocol.

Isolation and culture of primary murine BMDM

BMDMs were isolated from the femurs and tibias of 10-week-old C57BL/6 mice. Cells were plated on bacteriological plastic plates in macrophage growth medium consisting of RPMI-1640 (Invitrogen), 1×HEPES (Invitrogen), 5 mM penicillin/streptomycin (Invitrogen), and 10% heat-inactivated fetal bovine serum (Gibco) supplemented with 15% L-cell-conditioned medium as a source of CSF-1. After 1 day, nonadherent cells were collected, seeded at 8×10^5 cells/ml in bacteriological plates, and grown for 5 more days.

Western blot

Tissues and cells were lysed using RIPA buffer (50 mM Tris-HCl pH 7.4, 150 mM NaCl, 1% NP-40, 0.5% Na-deoxycholate, 0.1% SDS, 2 mM EDTA, and 50 mM NaF) supplemented with protease and phosphatase inhibitor cocktails (Roche / Thermo Fisher Scientific). Lysates were incubated on ice and cleared by centrifugation at 18,500 g for 15 minutes at 4°C. Protein concentration was determined by the Lowry method. Proteins were separated by SDS-PAGE and transferred onto polyvinylidene difluoride membranes. Proteins were detected using commercial antibodies against eIF2α, phospho-eIF2α (both from Cell Signaling), HSP90 (Santa Cruz), ASNS (Atlas antibodies), HSPA9 (Antibodies Online), LONP1 (Sigma), OXPHOS proteins (Total OXPHOS Rodent WB Antibody Cocktail, Abcam) and β-tubulin (Santa Cruz). Samples were analyzed by immunoblotting using standard procedures.

Microarray analysis and GSEA

Total RNA was isolated from flashfrozen and powdered liver and kidney aliquots using TRIzol (Life Technologies). RNA was purified using the RNeasy Mini Kit (Qiagen) in accordance with the manufacturer's instructions. Microarray analysis was performed using Affymetrix *mouse MTA1.0* chips in triplicates for each condition. Microarray data

was normalized with RMA-sketch method of the Affymetrix Expression console and analyzed using limma R package (56). Bonferroni adjusted p value<0.05 was used to determine the differentially expressed genes. GSEA was performed using the clusterProfiler package (57). Genesets in gmt format were obtained from the MSigDB Collections from the Broad Institute website. For each organ, all expressed genes were ordered by decreasing fold change based on the differential expression analysis upon Dox. We performed 10'000 permutations, a minimum gene set size of 10, and a maximum of 1000.

RNA-Seq analysis and GSEA analysis

RNA sequencing analysis was performed with extracted RNA from mouse tissues (Lungs, Liver & Kidneys) recovered at day 7 post intranasal infection with 175 PFU with influenza virus A (Influenza A/PR/8/34 (H1N1) originating from ATCC VR-1469) (n=5-6). RNA was extracted from flashfrozen, powedered tissue aliquots and cleaned using TRIzol reagent (Invitrogen) followed by Direct-zol-96 RNA kit (Zymo Research). RNA quality was assessed using Fragment Analyzer (Agilent). 1 ug of total RNA was used for the construction of sequencing libraries. For each sample, 60 million paired-end sequencing reads of length of 100 base pairs each were sequenced using DNBseq Eukaryotic-T resequencing (BGI Sequencing). FastQC (58) was used to verify the quality of the reads. No low-quality reads were present and no trimming was needed. Alignment was performed against mouse genome (CRCm38 mm10 primary assembly and Ensembl release 95 annotation) using STAR (version 2.73a) (59). The obtained STAR gene-counts for each alignment were analyzed for differentially expressed genes using the R packages edgeR (version 3.24.3) limma (version 3.38.3) (60) using a generalized-linear model. A threshold of 1 log2 fold change and adjusted P value smaller than 0.05 were considered when identifying the differentially expressed genes.

A principal component analysis (61) was used to explore the variability between the different samples. The RUVSeq (version 1.16.1) (62) Bioconductor R package was used to correct for the unwanted variation. We used the clusterProfiler R package to conduct GSEA analysis on gene ontology (GO) terms (57). We used a minimum gene set size of 10, a maximum gene set size of 500, and performed 10,000 permutations. We used a gene list ordered by log2(Fold Changes) from the differential expression analysis. The clusterProfiler (version 3.17.1) packages was used for GSEA and various data representations. ReviGO (41) was used to generate clustering of enrichment analysis results. The UpSetR package (63) was used for multi-group overlap.

qRT-PCR

RNA from cells and tissues was extracted using TRIzol and then reverse-transcribed into cDNA by the QuantiTect Reverse Transcription Kit (Qiagen) following the manufacturer's instructions. The qPCR reactions were performed using the LightCycler 480 II system and SYBR Green qPCR Master mix (Roche). All results are presented relative to the mean of *housekeeping genes* ($\Delta\Delta C_t$ method). All mRNA expression levels were corrected for expression of the housekeeping gene *36B4* or *Actb* for samples of mouse origin, *ACTB* for samples of human origin. A list of primers used is available in the supplemental material.

Origin or synthesis of the screened compounds

Structure, origin or synthesis method of the screened compound is indicated in the Table S3.

Quantification of mtDNA released into cytosol

After 1 hour of treatment with the indicated concentration of Dox, day 6-differentiated BMDM (a 10-cm cell culture for n=1) were harvested by gentle incubation in Cell dissociation Buffer (Gibco) (2 min at 37°C), harvested in a tube, briefly centrifuged (400g, 4 min) and rinsed once with PBS. Then, the assessment of cytosolic mtDNA was carried out as described and with the same primers as in (64).

IFNβ measurement in culture medium

BMDM at day 6 of differentiation were treated with the indicated concentrations of drugs in a controlled volume of culture medium for 16-24 hours. Culture medium was harvested and was assessed for IFNβ concentration using the VeriKine-HS Mouse Interferon Beta Serum ELISA kit (PBL assay Science) according to the manufacturer's instructions.

Compound screening in *C. elegans*

The strain used to assess UPR^{mt} activation was SJ4100 (zcIs13[*hsp-6*::GFP]) (25) and was provided by the Caenorhabditis Genetics Center (University of Minnesota). Worms were maintained on nematode growth medium (NGM) agar plates seeded with E.coli OP50 at 20 °C. Compound screening plates were obtained by dissolving each compound at 68 µM (except 9-TB at 17µM, for which the effect was too strong at higher concentrations) in NGM agar supplemented with carbenicillin (25mg/L) and IPTG (2mM) and seeded with HT115 RNAi control bacteria or with *cco-1* RNAi clone (F26E4.9). L4 larvae were transferred manually on the compound screening plates and fluorescence was assessed at day 1 of adulthood (similar exposure time for all images). The screening was performed at 20°C.

Viral titer

The lung viral titer was determined by plaque assay and the data are shown as Log 10 (plaques/ g tissue). The plaque assay was performed with the MDCK cells as follows: MDCK cells were seeded at the density of $2.5*10^5$ cells/mL. Lung samples were homogenised with tissue lyser II after thawing. After centrifugation, the lung homogenates were serially diluted with infection medium, 10-fold for 6 dilutions and pipetted to a 6-well plate. After incubation, the cell infection medium was replaced with infection medium containing 0.625% low-melting-point agarose. After fixation with 4% paraformaldehyde, cells were stained with 0.5% crystal violet solution. Plaques were counted visually and the virus titer was calculated as follows: virus titer/g lung tissue=Log 10 (plaques/well*dilution factor*1000).

Microbiota initial randomization and feces collection

The mouse microbiome was normalized across cages using a randomization and bedding mixing procedure. At day -17, 24 mice were randomized into 4 balanced groups to mix littermates: vehicle (health control), vehicle (infection control), and respectively 9-TB and Dox treated. The bedding of each cage was thereafter not changed for 4 consecutive days. On day -13, roughly half of the soiled bedding (with feces) of each cage were collected and mixed in equal amounts in a sterile container. Mice were then put in clean cages filled with half clean bedding and half pooled beddings. This procedure was repeated at the next cage change at day -8. Feces samples were then collected on day -4, day 0 (inoculation day and 3 days post Dox/9-TB treatment) and day 3 (3 days post infection and 6 days post Dox/9-TB treatment). Each time mice were single-caged without bedding for 2-4 hours and fresh feces were immediately collected and frozen on dry ice. Mice of vehicle, 9-TB and Dox groups were inoculated with influenza A virus on day 0 via intranasal route at the dose of 665

p.f.u./mouse/50 µL under general anesthesia by injection of anesthetic (Zoletil 50+Xylazine Hydrochloride, 30 mg/kg+6 mg/kg) on the day of inoculation (day 0). Mice in all groups were treated with vehicle (saline) or the indicated concentrations of Dox/9-TB by daily intraperitoneal injection from day -3 until the end of the experiment.

Whole metagenome sequencing

DNA was extracted using the MagMAX Microbiome Ultra Nucleic Acid Isolation Kit (Thermo Fisher, Catalog#: A42358) using 100 mg of fecal sample for 800 µL of Lysis Buffer. Bead beating was performed for 5 min at 50 Hz. Lysate was centrifuged at 14,000 g for 2 min and 400-500 µL of supernatant was used in subsequent steps using a KingFisher Flex system (Thermo Fisher) following the manufacturer's protocol. Extracted DNA was quantified using the Qubit dsDNA Assay Kit (Thermo Fisher). Sequencing library was prepared with 100 ng of DNA per sample. Briefly: Shearing was performed on a Covaris LE200 system, end repair, A-tailing, ligation of adaptors and PCR were performed using the KAPA Hyper Prep Kit (Roche, Catalog#: 07962363001) with the following PCR program: 45 min at 98 deg C, 7 cycles including 15 min at 98 deg C, 30 min at 60 deg C and 30 min at 72 deg C, then finally 60 min at 72 deg C and holding 4 deg C until samples retrieval.

Library concentration was measured using the Qubit dsDNA Assay Kit (Thermo Fisher) and fragment length was assessed on an Agilent TapeStation. The library was sequenced on an Illumina Novaseq6000 platform using paired-end 2x150 bp chemistry. Sequences were deposited on the European nucleotide archive (ENA) and are publicly available under accession number PRJEB52004.

Whole metagenome sequencing data analysis

Low quality bases and adapters were trimmed. Short reads (length <35 bp) and low-quality reads were removed. Host sequences were identified by mapping to the host reference genome with bowtie2 (65), then removed. Taxonomy was assigned using the the Kraken2 (66) sequence classifier with an in house developed microbial database including 27,165 reference genomes (spanning 9,471 bacteria, 1,854 fungi, 15,752 viruses, 88 parasites). Genus and species relative abundances in terms of reads per million (rpm) were estimated using Bracken (67). Statistical analysis of the fecal bacterial communities was performed in R and Rstudio. The entire code used in this analysis is publicly available on the GitHub repository https://github.com/auwerxlab/dox-9tb-mouse-metagenomic-analysis-01 and was archived on Zenodo (10.5281/zenodo.6759368). Briefly, the species composition of the bacterial communities was assessed using perMANOVA based on the Bray-Curtis dissimilarity and 10,000 permutations with p-values adjusted for multiple comparisons using the Benjamini and Hochberg method. Samples similarities were further assessed using NMDS analysis based on the Bray-Curtis dissimilarity. Bacterial species diversity was assessed in terms of Shannon diversity index (SDI) and richness and compared using Kruskal–Wallis one-way analysis of variance followed by post-hoc Wilcoxon tests with p-value adjusted for multiple comparison using the Holm-Bonferroni method. .

Statistics

Differences between two groups were assessed using two-tailed t tests. Differences between more than two groups were assessed with one-way analysis of variance (ANOVA), unless stated otherwise. For survival curves, statistical analysis was performed by Log-rank (Mantel-Cox) test. GraphPad Prism 6 was used for statistical analyses. Variability in plots and graphs is presented as standard error mean (SEM), unless stated otherwise. All $p \leq 0.05$ were considered to be significant. *$p \leq 0.05$; **p

≤ 0.01; ***p ≤ 0.001. Mouse experiments were performed once. IFV infection studies and the *C. elegans* screening were performed in a blinded manner. Calculation of sample sizes for worm, cell and animal experiments were determined based on previous findings. Sample sizes, replicates, and statistical methods are specified in the figure legends.

Study approval

In all studies animals' care was in accordance with institutional guidelines. The germ-free C57BL/6 animal experiment was carried out according to the institutional, national Swiss and EU ethical guidelines and were approved by the local animal experimentation committee of the Canton de Vaud (Service de la consommation et des affaires vétérinaires du Canton de Vaud, Epalinges (Switzerland); protocol VD2779.a). IFV-infection animal studies were performed according to the protocol following the institutional guidelines of Institutional Committee Animal Care and Use Committee, Shanghai Site (IACUC-SH; protocol ID01-031-2019v1.1) and approved by the Shanghai Science and Technology Committee (STCSM, Ministry of Science and Technology, PR of China). All animals that showed signs of severe illness, predefined by the animal authorization protocol before the start of the experiment, were euthanized.

Data and materials availability

All bioinformatic data associated with the study are present in the paper or the Supplementary Materials. The data discussed in this publication are being deposited in NCBI's Gene Expression Omnibus and are accessible under GEO Series accession number GSE174124 for RNA-Seq data and under GEO Series accession number GSE202754 for microarray data. Whole metagenome sequences were deposited on

624 the European nucleotide archive (ENA) and are publicly available under accession
625 number PRJEB52004.

626

627

Author contributions:

The study was conceived and designed by AM, MN, and JA. AM, TYL, EK, DL, LM, NLH and DD performed the in vitro, worm, and mouse experiments. MG and MN designed, synthesized and characterized the tetracycline derivatives. AR, GEL and AM performed the bioinformatics analysis. AM and JA wrote the manuscript with help of MN, and all authors gave critical comments. JA and MN supervised the work.

Acknowledgments:

We thank D. Ron (Cambridge Institute for Medical Research) for providing the *Atf4*$^{-/-}$ MEFs. We thank Marie Janod, Sabrina Bichet, Dr Norman Moullan, Dr Alessia Perino, Dr Ludger Goeminne, Dr Maroun Bou Sleiman, Dr Pedro M. Quirós, Dr Virginija Jovaisaite, Leo Diserens, Manuel Kulagin, the members of the Auwerx lab, the EPFL animal facilities, the EPFL FACS facility, the EPFL histology facility, and the UNIL genomics facility for help, advice and/or comments. **Funding:** The work was supported by the Ecole Polytechnique Fédérale de Lausanne (EPFL), and grants from the European Research Council (ERC-AdG-787702), the Swiss National Science Foundation (SNSF 31003A_179435), and a GRL grant of the National Research Foundation of Korea (NRF 2017K1A1A2013124). N.L.H. is supported by a National Health and Medical Research Council (NHMRC) of Australia SRF-B fellowship.

Conflict of interests

AM, MN and JA are inventors on a patent application filed by EPFL. MN and JA hold shares in Tiberius therapeutics. The other authors do not declare a conflict of interest.

References

1. Zhao Q et al. A mitochondrial specific stress response in mammalian cells. *The EMBO journal* 2002;21(17):4411–9.

2. Mottis A, Herzig S, Auwerx J. Mitocellular communication: Shaping health and disease. *Science* 2019;366(6467):827–832.

3. Shpilka T, Haynes CM. The mitochondrial UPR: mechanisms, physiological functions and implications in ageing. *Nature reviews. Molecular cell biology* [published online ahead of print: November 22, 2017]; doi:10.1038/nrm.2017.110

4. Bar-Ziv R, Bolas T, Dillin A. Systemic effects of mitochondrial stress. *EMBO reports* 2020;21(6):e50094.

5. Houtkooper RH et al. Mitonuclear protein imbalance as a conserved longevity mechanism. *Nature* 2013;497(7450):451–7.

6. Durieux J, Wolff S, Dillin A. The cell-non-autonomous nature of electron transport chain-mediated longevity. *Cell* 2011;144(1):79–91.

7. Sorrentino V et al. Enhancing mitochondrial proteostasis reduces amyloid-beta proteotoxicity. *Nature* [published online ahead of print: December 6, 2017]; doi:10.1038/nature25143

8. Wang YT et al. Cardioprotection by the mitochondrial unfolded protein response requires ATF5. *American Journal of Physiology-Heart and Circulatory Physiology* 2019;317(2):H472–H478.

9. Moullan N et al. Tetracyclines Disturb Mitochondrial Function across Eukaryotic Models: A Call for Caution in Biomedical Research. *Cell reports* [published online ahead of print: March 10, 2015]; doi:10.1016/j.celrep.2015.02.034

10. Mills EL, Kelly B, O'Neill LAJ. Mitochondria are the powerhouses of immunity. *Nature immunology* 2017;18(5):488–498.

11. Pellegrino MW et al. Mitochondrial UPR-regulated innate immunity provides resistance to pathogen infection. *Nature* 2014;516(7531):414–7.

12. West AP et al. Mitochondrial DNA stress primes the antiviral innate immune response. *Nature* 2015;520(7548):553–7.

13. Tiku V, Tan M-W, Dikic I. Mitochondrial Functions in Infection and Immunity. *Trends in Cell Biology* 2020;30(4):263–275.

14. Colaço HG et al. Tetracycline Antibiotics Induce Host-Dependent Disease Tolerance to Infection. *Immunity* 2021;54(1):53-67.e7.

15. Almeida L et al. Ribosome-Targeting Antibiotics Impair T Cell Effector Function and Ameliorate Autoimmunity by Blocking Mitochondrial Protein Synthesis. *Immunity* 2021;54(1):68-83.e6.

16. Iwasaki A, Pillai PS. Innate immunity to influenza virus infection. *Nature Reviews Immunology* 2014;14(5):315–328.

17. Flerlage T, Boyd DF, Meliopoulos V, Thomas PG, Schultz-Cherry S. Influenza virus and SARS-CoV-2: pathogenesis and host responses in the respiratory tract. *Nature Reviews Microbiology* 2021;1–17.

18. Singer M. The role of mitochondrial dysfunction in sepsis-induced multi-organ failure. *Virulence* 2014;5(1):66–72.

19. Matthay MA et al. Acute respiratory distress syndrome. *Nat Rev Dis Primers* 2019;5(1):18.

20. Subramanian A et al. Gene set enrichment analysis: A knowledge-based approach for interpreting genome-wide expression profiles. *PNAS* 2005;102(43):15545–15550.

21. Quiros PM et al. Multi-omics analysis identifies ATF4 as a key regulator of the mitochondrial stress response in mammals. *The Journal of cell biology* 2017;216(7):2027–2045.

22. D'Amico D, Sorrentino V, Auwerx J. Cytosolic Proteostasis Networks of the Mitochondrial Stress Response. *Trends in biochemical sciences* 2017;42(9):712–725.

23. Emming S, Schroder K. Tiered DNA sensors for escalating responses. *Science* 2019;365(6460):1375–1376.

24. Nelson I, Hanna MG, Wood NW, Harding AE. Depletion of mitochondrial DNA by ddC in untransformed human cell lines. *Somat Cell Mol Genet* 1997;23(4):287–290.

25. Yoneda T et al. Compartment-specific perturbation of protein handling activates genes encoding mitochondrial chaperones. *Journal of cell science* 2004;117(Pt 18):4055–66.

26. Nelson ML et al. Inhibition of the tetracycline efflux antiport protein by 13-thio-substituted 5-hydroxy-6-deoxytetracyclines. *J Med Chem* 1993;36(3):370–377.

27. Nelson ML et al. Versatile and Facile Synthesis of Diverse Semisynthetic Tetracycline Derivatives via Pd-Catalyzed Reactions. *J. Org. Chem.* 2003;68(15):5838–5851.

28. Honeyman L et al. Structure-Activity Relationship of the Aminomethylcyclines and the Discovery of Omadacycline. *Antimicrob Agents Chemother* 2015;59(11):7044–7053.

29. Sum PE et al. Glycylcyclines. 1. A new generation of potent antibacterial agents through modification of 9-aminotetracyclines. *J Med Chem* 1994;37(1):184–188.

30. Stephens CR et al. The Structure of Aureomycin1. *J. Am. Chem. Soc.* 1954;76(13):3568–3575.

31. Stephens CR et al. 6-Deoxytetracyclines. IV.1,2 Preparation, C-6 Stereochemistry, and Reactions. *J. Am. Chem. Soc.* 1963;85(17):2643–2652.

32. Bernardi L, de Castiglione R, Colonna V, Masi P, Mazzoleni R. Tetracycline derivatives I. Esters of 5-oxytetracyclines: chemistry and biological activity. *Farmaco Sci* 1974;29(12):902–909.

33. Atakan HB, Cornaglia M, Mouchiroud L, Auwerx J, Gijs MAM. Automated high-content phenotyping from the first larval stage till the onset of adulthood of the nematode Caenorhabditis elegans. *Lab Chip* 2018;19(1):120–135.

34. Bastos LFS et al. A novel non-antibacterial, non-chelating hydroxypyrazoline derivative of minocycline inhibits nociception and oedema in mice. *Br J Pharmacol* 2008;155(5):714–721.

35. Nelson M, Hillen W, Greenwald RA (eds). *Tetracyclines in Biology, Chemistry and Medicine [Internet]*. Basel: Birkhäuser Basel; 2001:

724 36. Moriyama M, Koshiba T, Ichinohe T. Influenza A virus M2 protein triggers mitochondrial DNA-
725 mediated antiviral immune responses. *Nat Commun* 2019;10(1):4624.

726 37. Chung HK et al. GDF15 deficiency exacerbates chronic alcohol- and carbon tetrachloride-induced
727 liver injury. *Scientific Reports* 2017;7(1):17238.

728 38. Zhang J-Y et al. Single-cell landscape of immunological responses in patients with COVID-19.
729 *Nature Immunology* 2020;21(9):1107–1118.

730 39. Khan NA et al. mTORC1 Regulates Mitochondrial Integrated Stress Response and Mitochondrial
731 Myopathy Progression. *Cell Metab* 2017;26(2):419-428.e5.

732 40. Zaim S, Chong JH, Sankaranarayanan V, Harky A. COVID-19 and Multiorgan Response. *Current*
733 *Problems in Cardiology* 2020;45(8):100618.

734 41. Supek F, Bošnjak M, Škunca N, Šmuc T. REVIGO summarizes and visualizes long lists of gene
735 ontology terms. *PLoS One* 2011;6(7):e21800.

736 42. Steuerman Y et al. Dissection of Influenza Infection In Vivo by Single-Cell RNA Sequencing. *Cell*
737 *Systems* 2018;6(6):679-691.e4.

738 43. Angelidis I et al. An atlas of the aging lung mapped by single cell transcriptomics and deep tissue
739 proteomics. *Nature Communications* 2019;10(1):963.

740 44. Galani I-E et al. Untuned antiviral immunity in COVID-19 revealed by temporal type I/III interferon
741 patterns and flu comparison. *Nature Immunology* 2021;22(1):32–40.

742 45. West AP, Shadel GS. Mitochondrial DNA in innate immune responses and inflammatory
743 pathology. *Nature reviews. Immunology* 2017;17(6):363–375.

744 46. Jovanovic M et al. Dynamic profiling of the protein life cycle in response to pathogens [Internet].
745 *Science* 2015;347(6226). doi:10.1126/science.1259038

746 47. Kissig M et al. PRDM16 represses the type I interferon response in adipocytes to promote
747 mitochondrial and thermogenic programing. *The EMBO Journal* 2017;36(11):1528–1542.

748 48. Beilharz MW, Cummins JM, Bennett AL. Protection from lethal influenza virus challenge by oral
749 type 1 interferon. *Biochemical and Biophysical Research Communications* 2007;355(3):740–744.

750 49. Davidson S, Crotta S, McCabe TM, Wack A. Pathogenic potential of interferon αβ in acute
751 influenza infection. *Nature Communications* 2014;5(1):3864.

752 50. Hadjadj J et al. Impaired type I interferon activity and inflammatory responses in severe COVID-19
753 patients. *Science* 2020;369(6504):718–724.

754 51. Wang N et al. Retrospective Multicenter Cohort Study Shows Early Interferon Therapy Is
755 Associated with Favorable Clinical Responses in COVID-19 Patients. *Cell Host Microbe*
756 2020;28(3):455-464.e2.

757 52. Major J et al. Type I and III interferons disrupt lung epithelial repair during recovery from viral
758 infection. *Science* 2020;369(6504):712–717.

759 53. Channappanavar R et al. Dysregulated Type I Interferon and Inflammatory Monocyte-Macrophage
760 Responses Cause Lethal Pneumonia in SARS-CoV-Infected Mice. *Cell Host Microbe* 2016;19(2):181–
761 193.

762 54. Balducci C, Forloni G. Doxycycline for Alzheimer's Disease: Fighting β-Amyloid Oligomers and
763 Neuroinflammation [Internet]. *Front Pharmacol* 2019;10. doi:10.3389/fphar.2019.00738

764 55. Lindeman Jan H.N., Abdul-Hussien Hazem, van Bockel J. Hajo, Wolterbeek Ron, Kleemann
765 Robert. Clinical Trial of Doxycycline for Matrix Metalloproteinase-9 Inhibition in Patients With an
766 Abdominal Aneurysm. *Circulation* 2009;119(16):2209–2216.

767 56. Ritchie ME et al. limma powers differential expression analyses for RNA-sequencing and
768 microarray studies. *Nucleic acids research* 2015;43(7):e47.

769 57. Yu G, Wang LG, Han Y, He QY. clusterProfiler: an R package for comparing biological themes
770 among gene clusters. *Omics : a journal of integrative biology* 2012;16(5):284–7.

771 58. Babraham Bioinformatics - FastQC A Quality Control tool for High Throughput Sequence Data
772 [Internet]https://www.bioinformatics.babraham.ac.uk/projects/fastqc/. cited May 10, 2021

773 59. Dobin A et al. STAR: ultrafast universal RNA-seq aligner. *Bioinformatics* 2013;29(1):15–21.

774 60. Robinson MD, McCarthy DJ, Smyth GK. edgeR: a Bioconductor package for differential
775 expression analysis of digital gene expression data. *Bioinformatics* 2010;26(1):139–140.

776 61. Lê S, Josse J, Husson F. FactoMineR: An R Package for Multivariate Analysis. *Journal of*
777 *Statistical Software* 2008;25:1–18.

778 62. Risso D, Ngai J, Speed TP, Dudoit S. Normalization of RNA-seq data using factor analysis of
779 control genes or samples. *Nature Biotechnology* 2014;32(9):896–902.

780 63. Conway JR, Lex A, Gehlenborg N. UpSetR: an R package for the visualization of intersecting sets
781 and their properties. *Bioinformatics* 2017;33(18):2938–2940.

782 64. Kim J et al. VDAC oligomers form mitochondrial pores to release mtDNA fragments and promote
783 lupus-like disease. *Science* 2019;366(6472):1531–1536.

784 65. Langmead B, Salzberg SL. Fast gapped-read alignment with Bowtie 2. *Nat Methods*
785 2012;9(4):357–359.

786 66. Wood DE, Lu J, Langmead B. Improved metagenomic analysis with Kraken 2. *Genome Biology*
787 2019;20(1):257.

788 67. Lu J, Breitwieser FP, Thielen P, Salzberg SL. Bracken: estimating species abundance in
789 metagenomics data. *PeerJ Comput. Sci.* 2017;3:e104.

790

791

Figures

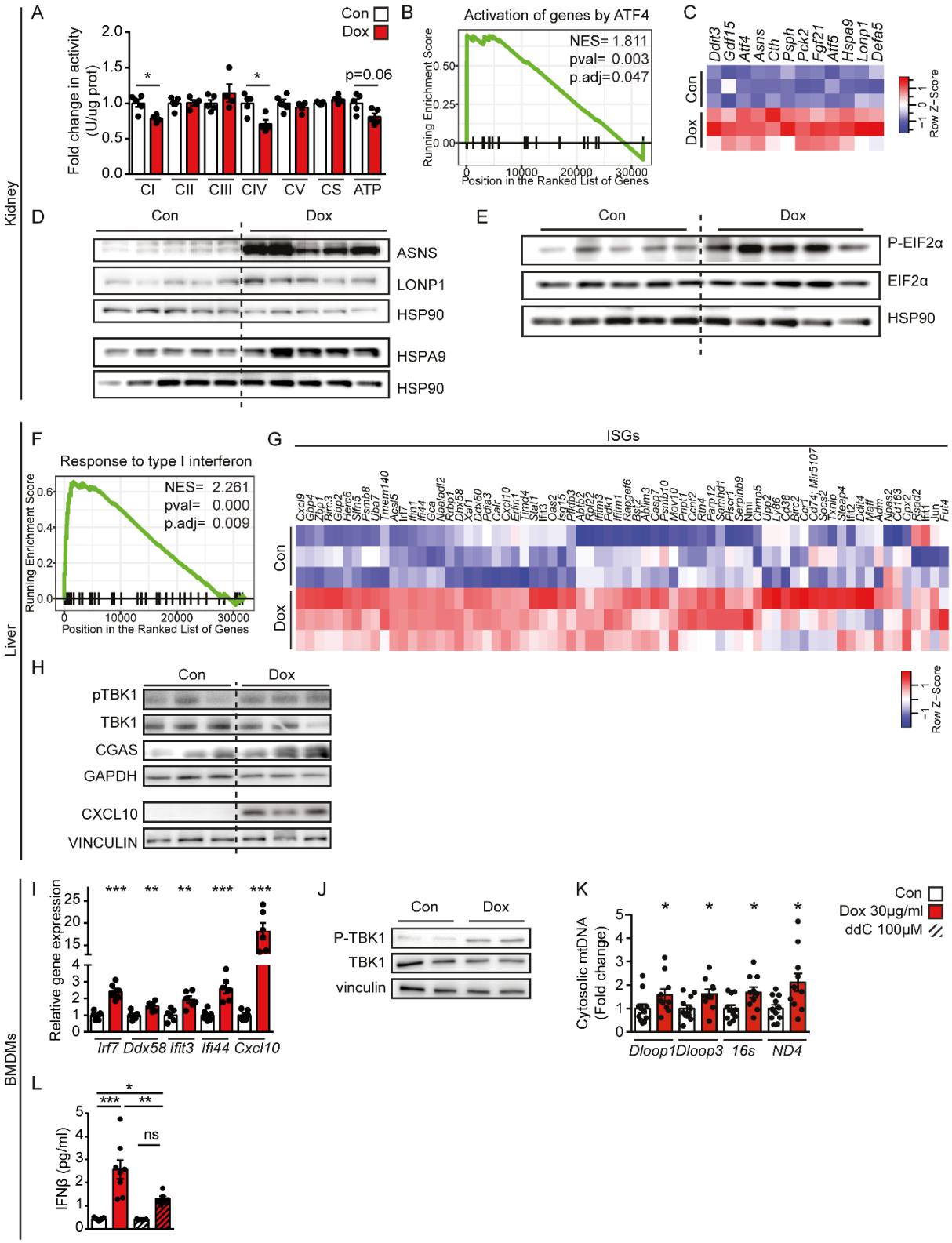

Figure 1: Doxycycline induces the ATF4 response and the type I IFN response.

A. Biochemical measurement of oxidative phosphorylation (OXPHOS) complexes and ATP levels in the kidney of germ-free C57BL/6J male mice raised and maintained in a germ-free

environment and that were drinking regular water or water supplemented with doxycycline (Dox) at 500 mpkd for 16 days (n=4-5). **B-C**. Enrichment score plot for the gene set “Reactome Activation of genes by ATF4” (B) and heatmap representing the transcript levels of ATF4/5 targets (C) from kidney transcriptomics data of control vs Dox-treated germ-free mice. **D**. Western blot analysis of selected ATF4 targets in the kidneys of germ-free mice (corresponding loading control below, HSP90). **E**. Immunoblots of phosphorylated EIF2α (P-EIF2α) and total EIF2α (E) in kidneys of Dox-treated germ-free mice. **F-G**. Enrichment score plot for the GO term “Response to type I interferon” (F) and heatmap representing the transcript levels of some interferon-stimulated genes (ISGs) (G) from livers of germ-free mice treated with Dox. **H.** Immunoblots of phosphorylated TBK1 (pTBK1), TBK1, the ISG proteins, CGAS and CXCL10, (corresponding loading control below, resp. VINCULIN and GAPDH). **I**. Transcript levels of selected ISGs of bone marrow-derived macrophages (BMDM) (day 6 of differentiation, derived from C57BL/6J mice) treated with Dox at 30μg/ml for 9 hours (n=6). **J**. Immunoblots of phosphorylated TBK1 (pTBK1), TBK1, and vinculin as control in BMDM treated with Dox at 30μg/ml for 3 hours. **K**. Amplification of different mtDNA regions by qPCR in the cytosolic fraction of BMDMs with Dox at 30μg/ml for 1 hour (n=10). **L**. Levels of interferon β (IFNβ) in the culture medium of BMDM treated with Dox (30μg/ml for 14 hours) and/or 2',3' dideoxycytidine (ddC at 100μM for 72 hours) (n=8). Statistical analysis: Wilcoxon test p-values corrected for multiple comparisons with Hommel’s method (A, I, K) or by one-way ANOVA followed by Tukey post-hoc correction (L) (*$p \leq 0.05$, **$p \leq 0.01$, ***$p \leq 0.001$). Error bars represent standard error mean (SEM).

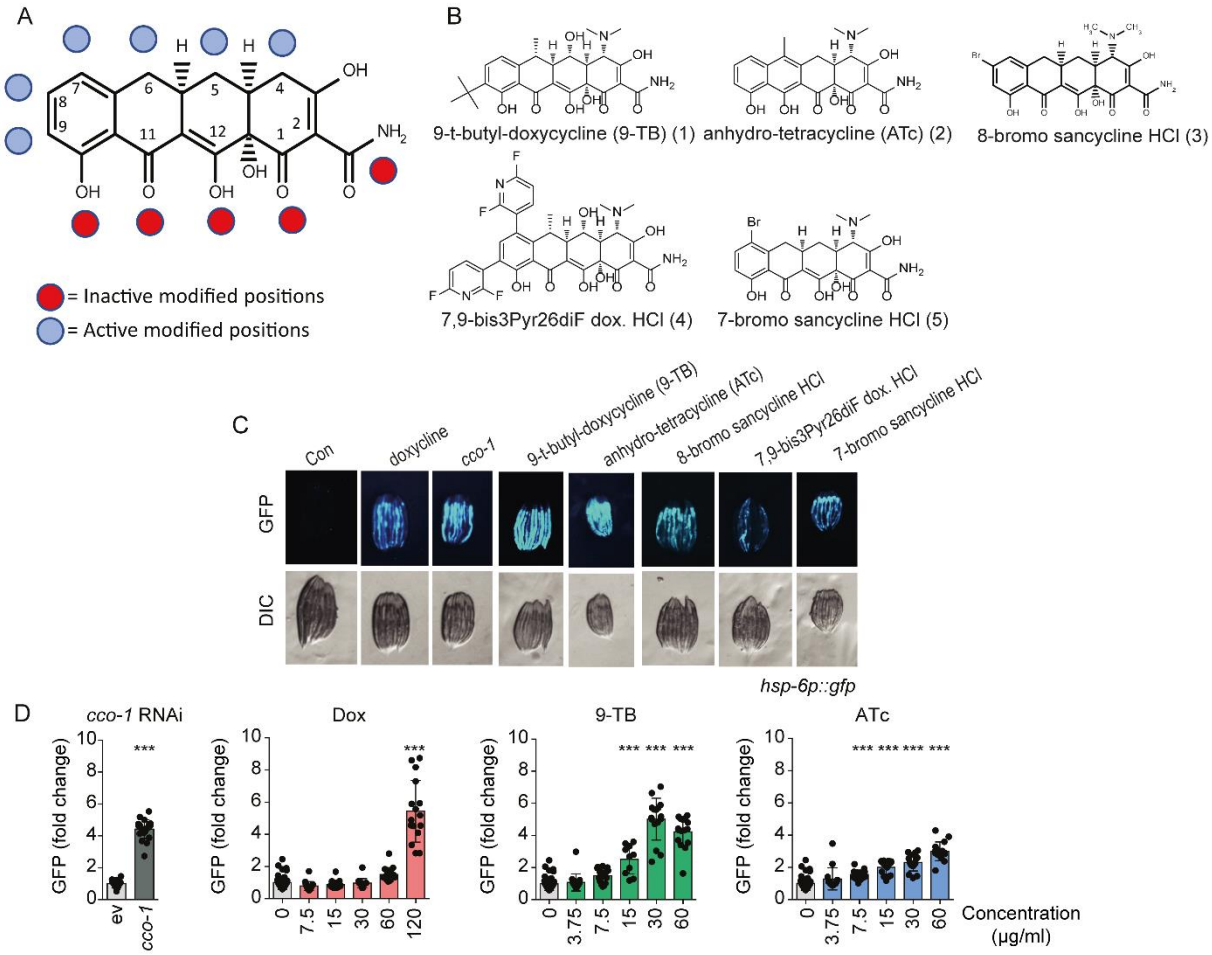

818

819 **Figure 2: Selecting Tet derivatives that induce UPR^{mt} in *C. elegans.***

820 **A**. Structural locants of the Tet scaffold and UPR^{mt}-active and -inactive compounds by
821 chemically modified positions (based on activity of the *hsp-6::gfp* reporter, Fig. 2C). **B**.
822 Chemical structures of the Tet derivatives shown in Fig.2A-B. **C**. Representative images of the
823 induction of the UPR^{mt} in the *C. elegans hsp-6::gfp* reporter strain (25) exposed to the indicated
824 tetracycline derivatives at 68 µM (except for 9-TB, which is at 17 µM) since the parental L4
825 stage. Dox and OXPHOS LOF through feeding *cco-1* RNAi serve as positive controls. The
826 pictures show the progeny at day 2-3 of adulthood (similar exposure time for all images; GFP-
827 fluorescence in top raw, differential interference contrast (DIC) in bottom raw). **D.** Dose-
828 response for the UPR^{mt} activation (*hsp-6::gfp* reporter strain) upon exposure to different
829 concentrations of Dox, 9-TB, ATc or treatment with *cco-1* RNAi using an automated microfluidic
830 device (33) (n=14-16). Statistical analysis was performed by one-way ANOVA followed by
831 Bonferroni post-hoc correction (*$p \leq 0.05$, **$p \leq 0.01$, ***$p \leq 0.001$). Error bars represent
832 standard deviation (SD).

833

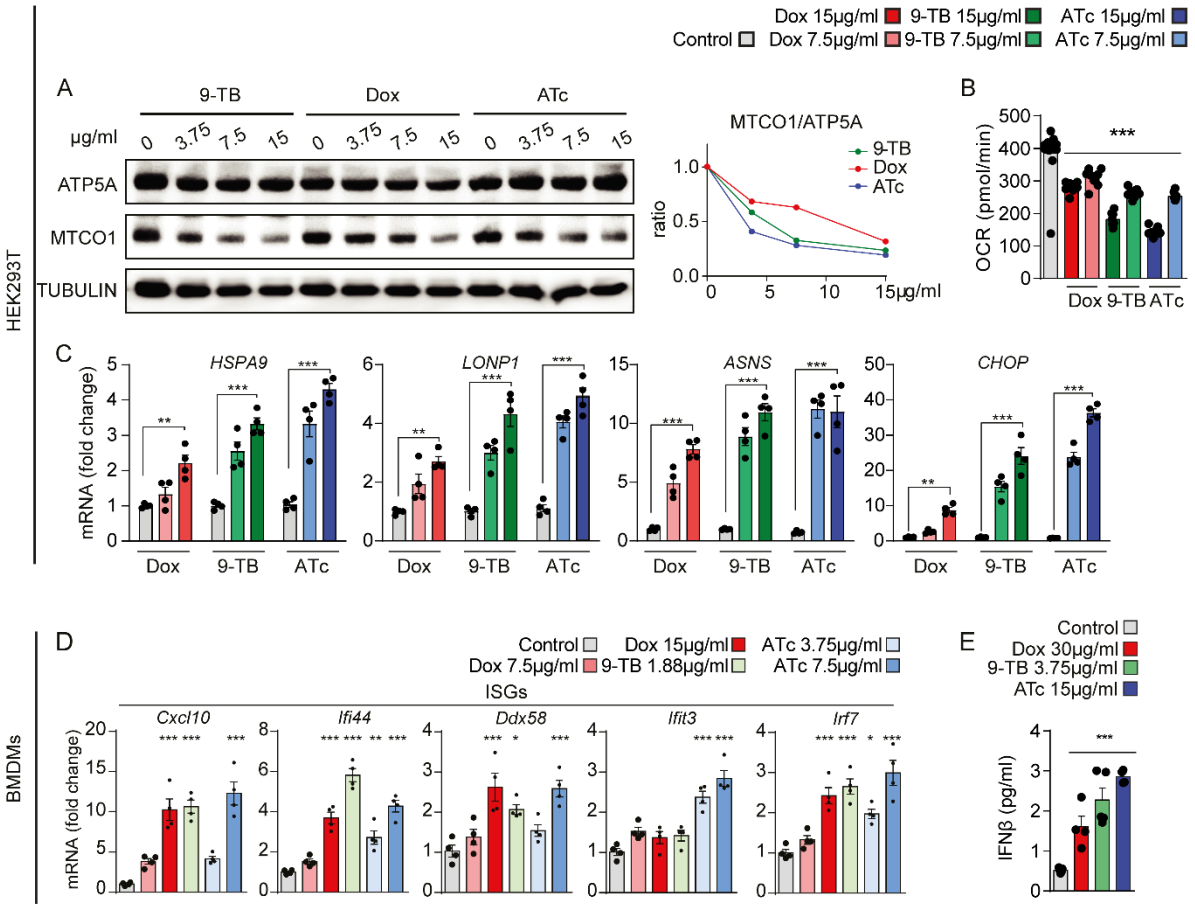

834

835 **Figure 3: Tet derivatives induce the MSR and type I IFN signalling in mammalian**
836 **cells.**

837 **A-C**. Tet derivatives induce a mito-nuclear protein imbalance and the MSR in human HEK293T
838 cells treated for 24 hours at the indicated concentrations. **A**. Immunoblots of HEK293T cells
839 for the OXPHOS subunits ATP5A (encoded in nuclear DNA) and MTCO1 (encoded in
840 mitochondrial DNA) with TUBULIN serving as a control. Quantification of the relative
841 MTCO1/ATP5A ratio is shown on the right. **B**. Oxygen consumption rate of HEK293T cells
842 exposed to different concentrations of Dox, 9-TB, or ATc (n=8). **C**. Transcript levels of the
843 indicated MSR genes measured by RT-qPCR (n=4). **D-E**. Tet derivatives induce transcript
844 levels of the indicated ISGs (D) and stimulate IFNβ secretion (E) after 24 hours treatment at
845 the indicated concentrations in mouse BMDM (day 6 differentiation) (n=4). Statistical analysis
846 was performed by ANOVA followed by Tukey post-hoc test (*$p \leq 0.05$,**$p \leq 0.01$, ***$p \leq 0.001$).
847 Error bars represent standard error mean (SEM).

848

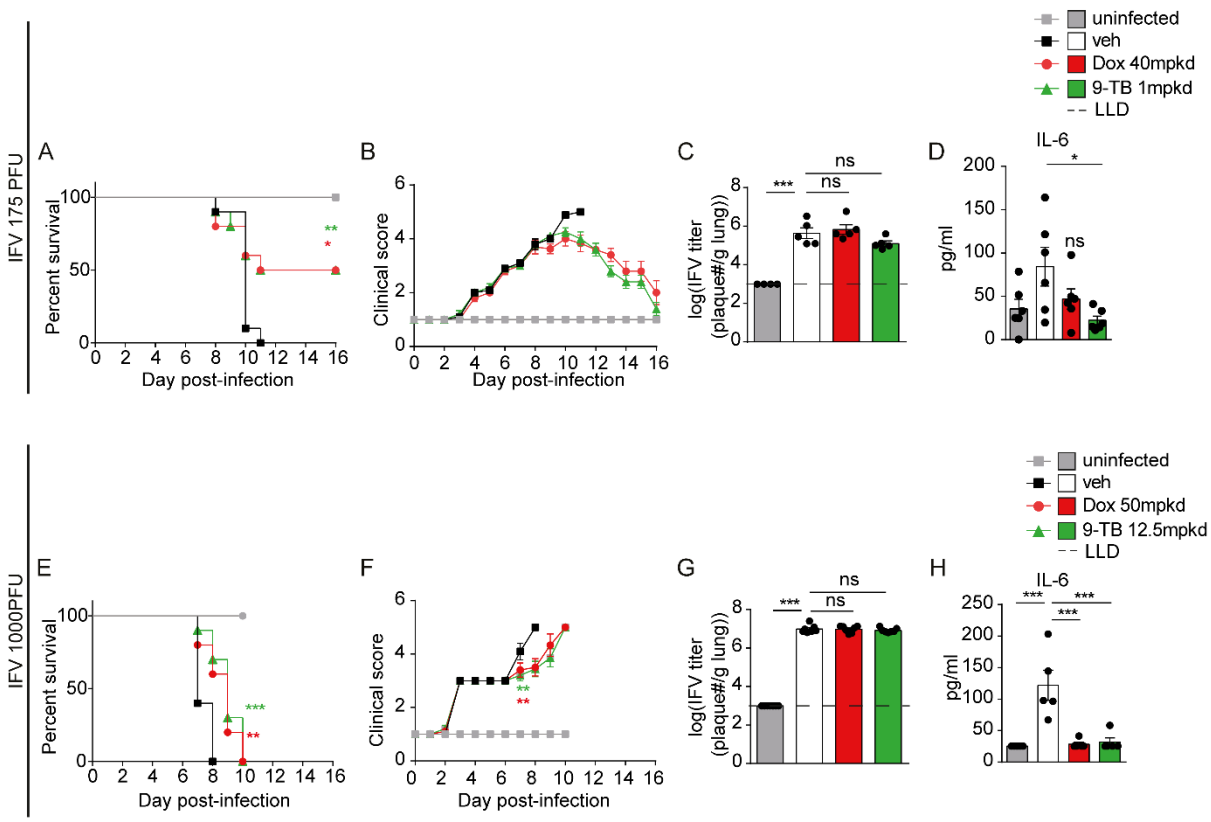

Figure 4: Tets mediate disease tolerance to IFV in mice.

A-D. 8-weeks old BALB/cN mice were injected with Dox (40 mpkd) or 9-TB (1 mpkd) and intranasally infected with 175 PFU of IFV-A H1N1 PR8, as described in Fig. S4A. Survival (A) and clinical score (B) were followed for 16 days post-infection (n=10). At day 7 post-infection, viral titers in lung lysates (C, n=5) and IL-6 levels in plasma (D, n=6) were measured (n=5). **E-H**. 8-weeks old BALB/cN mice were injected with Dox (50 mpkd) or 9-TB (12.5 mpkd) and intrasanally infected with 1000 PFU of IFV-A H1N1 PR8, as shown in Fig. S4B. Survival (E) and clinical score (F) were followed over 10 days post-infection (n=10). At day 5 post-infection, viral titers in lung lysates (G) and IL-6 levels in plasma (H) were measured (n=5). Statistical analysis was performed by ANOVA followed by Tukey post-hoc test (*p≤0.05,**p ≤ 0.01, ***p ≤ 0.001). For survival curves, statistical analysis was performed by Log-rank (Mantel-Cox) test (*p ≤ 0.05,**p ≤ 0.01, ***p ≤ 0.001). Error bars represent standard error mean (SEM).

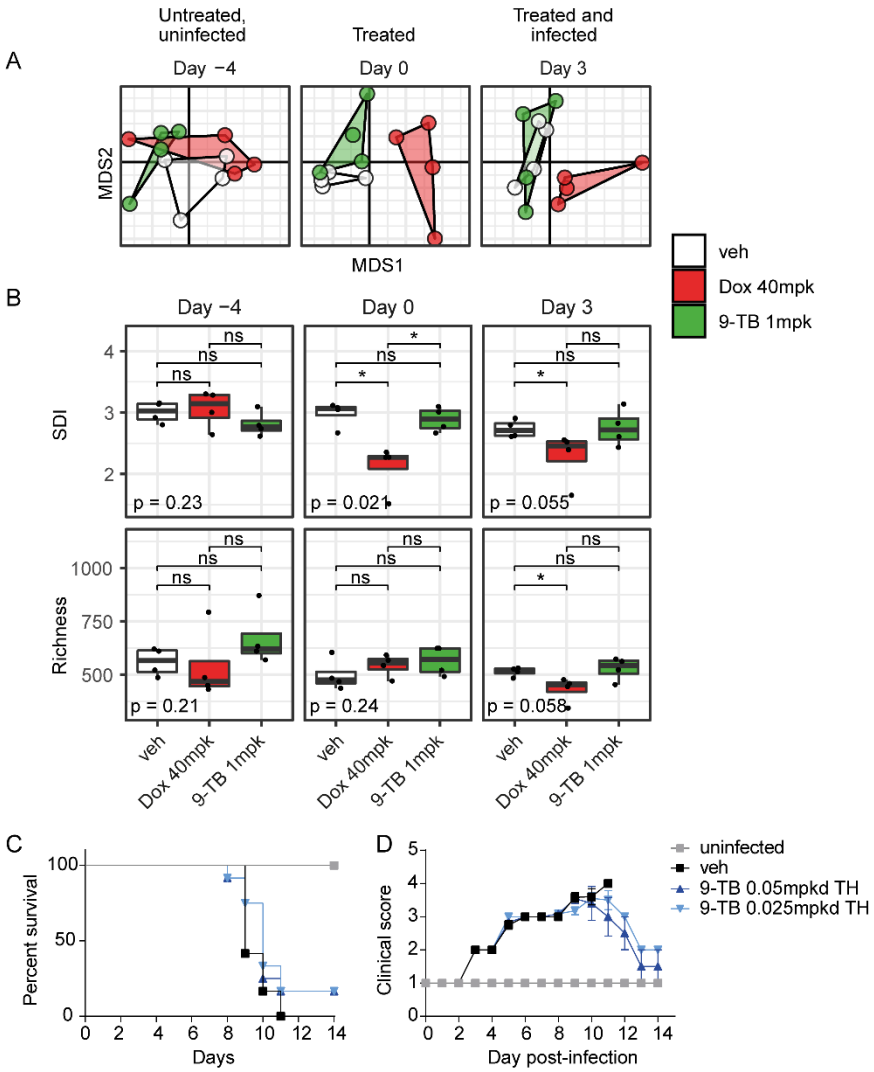

Figure 5: 9-TB does not impact gut microbiome and shows encouraging effects when therapeutically administered.

A. Comparison of bacterial community composition by nonmetric multidimensional scaling (NMDS) based on the Bray-Curtis dissimilarity. **B.** Comparison of bacterial species diversity in terms of Shannon diversity index (SDI) and richness. The lower and upper hinges are the first and third quartiles. The middle line is the median. The upper and lower whiskers respectively represent the highest and lowest values that are within 1.5x IQR from the hinge, where IQR is the inter-quartile range (i.e. distance between the first and third quartile). Data points beyond whiskers are considered outliers. Statistical significance assessed by Kruskal-Wallis test and post-hoc Wilcoxon test with p-value adjusted for multiple comparison using the Holm-Bonferroni method. '****': $p < 0.0001$, '***': $p < 0.001$, '**': $p < 0.01$, '*': $p < 0.05$, 'ns': $p > 0.05$. **C-D**. 8-weeks old BALB/cN mice (n=12) were infected intranasally with 760 PFU of IFV-A H1N1 PR8 and injected with 9-TB (0.05, 0.025 mpkd), as described in Fig. S5A. Survival (C) and clinical score (D) were followed for 14 days post-infection (n=12). Statistical analysis was performed by ANOVA followed by Tukey post-hoc test (*$p \leq 0.05$,**$p \leq 0.01$, ***$p \leq 0.001$). For survival curves, statistical analysis was performed by Log-rank (Mantel-Cox) test (*$p \leq 0.05$,**$p \leq 0.01$, ***$p \leq 0.001$). Error bars represent standard error mean (SEM).

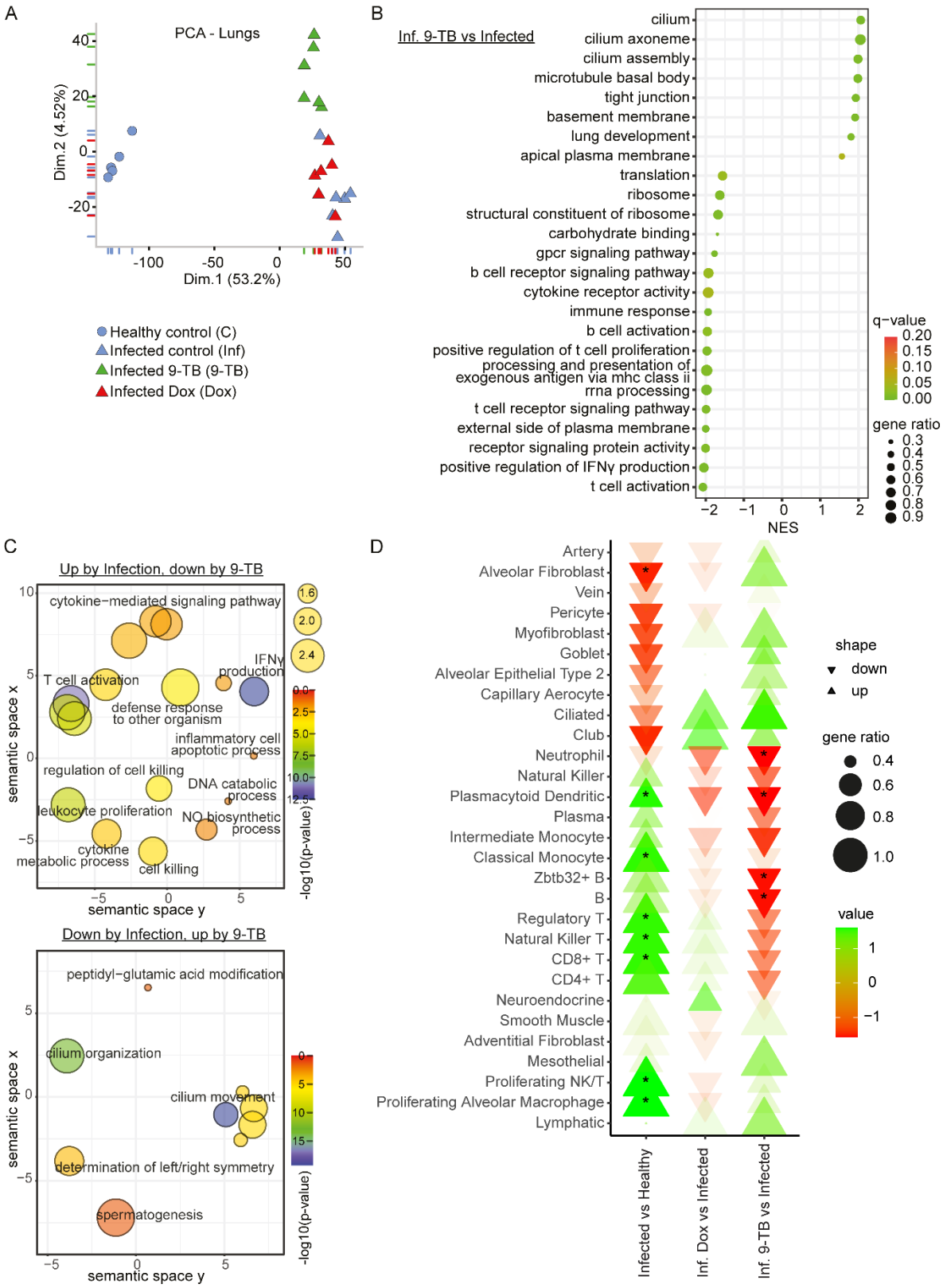

Figure 6: 9-TB counteracts the inflammatory and lung damaging effects of IFV infection.

A. Principal component analysis (PCA) of lung RNAseq transcriptomes collected at day 7 post-infection of BALB/cN mice with 175 PFU IFV-A H1N1 PR8 (n=5-6). **B**. Gene set enrichment

886 analysis (GSEA) results for Gene Ontology (GO) gene sets modulated in the comparison
887 between 9-TB treated versus control IFV-infected mice. A positive, respectively negative,
888 normalized enrichment score (NES) corresponds to an overall up-regulation, respectively
889 down-regulation, of the corresponding gene set. **C**. Revigo plot summarizing the main themes
890 in the significantly enriched GO Biological Process (GOBP) sets amongst genes induced by
891 IFV infection and down-regulated by 9-TB (left panel), and genes down-regulated by IFV
892 infection and induced by 9-TB (right panel).The size of the bubbles (top right legend) is
893 proportional to the number of annotations for the GO term (i.e. frequency) in the GO annotation
894 database, more general terms displaying larger bubbles. **D.** GSEA results of the RNA-Seq
895 data showing the directionality (increase or decrease) of the modulated lung cell transcript
896 profiles based on common markers shared by both human and mouse lung cell types derived
897 from extant single cell transcriptomic data (43). The alpha value (transparency) represents the
898 -log10(adjusted p-value) of the enrichment. * represents adjusted p-value < 0.05.

899

	Bacterial strains				
Compound	*E. coli*	*P. aeruginosa*	*K. pneumoniae*	*S. aureus*	*E. faecalis*
7- Br sancycline	8	4	1	0.5	0.5
8-Br sancycline	16	4	1	1	1
7,9-(bis-3'pyridinyl-2,4-diF)-sancycline	32	>64	8	8	4
9-t-butyl doxycycline (9-TB)	32	>64	>64	0.25	0.125
Anhydrotetracycline (ATc)	1	>64	8	1	1
Doxycycline	64	4	1	<0.125	<0.125
Minocycline	8	2	1	<0.125	<0.125

Table 1: Minimum Inhibitory Concentrations (µg/mL) of bacterial growth for indicated Tet derivatives and bacterial strains. All compounds were tested as the HCl salt forms. Strains specifications: *E. coli ATCC25922, P. aeruginosa ATCC27853, K. pneumoniae ATCC13883, S. aureus ATCC12600, E. faecalis ATCC19433.*

Supplemental Material :

Supplementary Methods

Supplementary Figures:

Figure S1: Doxycycline induces the ATF4 and the type I IFN response.

Figure S2: Dose-dependent effects of Tet derivatives on the UPR^{mt}.

Figure S3: Tet derivatives induce MSR genes in mammalian cells.

Figure S4: Tets mediate disease tolerance to IFV in mice.

Figure S5: Tets mediate disease tolerance to IFV in mice. (continued)

Figure S6: 9-TB counteracts the inflammatory and lung damaging effects of IFV infection.

Figure S7: 9-TB counteracts the inflammatory and lung damaging effects of IFV infection. (continued)

Supplementary tables:

Table S1: Differential expression results of liver and kidney microarrays from germ-free mice

Table S2: GSEA results of liver and kidney microarrays from germ-free mice

Table S3: Screened tetracycline derivatives

Table S4: Differential expression results in lungs of IFV-infected mice

Table S5: GSEA results in lungs, liver and kidneys of IFV-infected mice

Table S6: Differential expression results in kidneys and liver of IFV-infected mice

Table S7: Summary of domains relative representation per sample in whole metagenome sequencing reads.

Table S8: Comparison of bacterial community composition by permutational multivariate analysis of variance (perMANOVA) based on the Bray-Curtis dissimilarity with 10000 permutations. P-values adjusted for multiple comparisons using the Benjamini and Hochberg method. '****': $p < 0.0001$/ p.adj < 0.001, '***': $p < 0.001$/p.adj < 0.01, '**': $p < 0.01$/p.adj < 0.05, '*': $p < 0.05$/p.adj < 0.1, 'ns': $p > 0.05$/p.adj > 0.1.